Spin-orbit coupling and magnetic interactions in Si(111):{C,Si,Sn,Pb}

D. I. Badrtdinov,[1] S. A. Nikolaev,[1] M. I. Katsnelson,[1,2] and V. V. Mazurenko[1]
[1]*Theoretical Physics and Applied Mathematics Department, Ural Federal University, 620002 Ekaterinburg, Russia*
[2]*Institute for Molecules and Materials, Radboud University, Heyendaalseweg 135, 6525 AJ Nijmegen, The Netherlands*
(Received 24 September 2016; revised manuscript received 28 November 2016; published 19 December 2016)

We study the magnetic properties of the adatom systems on a semiconductor surface Si(111):{C,Si,Sn,Pb}-($\sqrt{3} \times \sqrt{3}$). On the basis of all-electron density functional theory calculations we construct effective low-energy models taking into account spin-orbit coupling and electronic correlations. The Hartree-Fock simulations for the unit cell with nine correlated orbitals put forward insulating ground states with the noncollinear 120°-Néel (for C, Si, Sn monolayer coverages) and 120°-row-wise (for Pb adatom) antiferromagnetic orderings. The corresponding spin Hamiltonians with anisotropic exchange interactions are derived by means of the superexchange theory and the calculated Dzyaloshinskii-Moriya interactions in the systems with Sn and Pb adatoms are revealed to be very strong and compatible with the isotropic exchange couplings. To simulate the excited magnetic states we solve the constructed spin models by means of the Monte Carlo method, where at low temperatures and zero magnetic field we observe complex spin spiral patterns in Sn/Si(111) and Pb/Si(111). On this basis the formation of antiferromagnetic skyrmion lattice states at high magnetic fields in the adatom *sp* electron systems is discussed.

DOI: 10.1103/PhysRevB.94.224418

I. INTRODUCTION

There is a special focus on the adatom systems Si(111):{C,Si,Sn,Pb}-($\sqrt{3} \times \sqrt{3}$) formed by a silicon surface (111) with the 1/3 monolayer coverage by C, Si, Sn, or Pb adatoms. Being the physical realizations of the one-band Hubbard model on a triangular lattice, this family of the adatom materials demonstrates a remarkable variety of interesting physical properties. For instance, the scanning tunneling spectroscopy and photoemission spectroscopy experiments [1] on Sn/Si(111) demonstrated the isostructural metal-insulator transition at ∼60 K predicted by Profeta and Tosatti [2] on the basis of LSDA + U calculations. Another important phenomenon observed in the scanning tunneling microscopy experiments is a charge density wave state related to the redistribution of the valence electrons in the system [3,4].

On the theoretical side, the main efforts to describe the Si(111):{C,Si,Sn,Pb} surface nanostructures were concentrated on the construction and solution of minimal electronic models taking into account local and nonlocal Coulomb interactions [2,5–9]. These studies successfully reproduced experimentally observed metal-insulator transitions and charge-ordering phase diagrams. Moreover, numerical simulations of the many-body Hamiltonians helped to resolve the existing discrepancies in various experiments suggesting different ordering phenomena [10].

Much less attention has been paid to the magnetic properties of these materials. At the moment there is no consistent description of the magnetic ground state as well as of the excited states at finite temperatures and magnetic fields. For instance, first-principles simulations [9] of the adatom system with Sn revealed that the 120° antiferromagnetic state has the lowest total energy, although it was shown that the magnetic moments are strongly delocalized. In turn, the authors of Ref. [7] reported on the formation of the so-called collinear row-wise magnetic ordering in the Sn/Si(111) system stabilized due to hopping processes beyond nearest neighbors. Such a magnetic model was motivated by the comparison of the angle-resolved photoemission spectroscopy (ARPES) experiment and dynamical cluster approximation spectra. However, there is still no direct experimental confirmation of the row-wise magnetic state. Last but not least, spin-orbit coupling was not taken into account in these studies. However, it can be very important and lead to nontrivial topological properties as it follows from the DFT results for Si/Si(111) presented in Ref. [11]. The situation with spin-orbit coupling can be even more interesting in the case of heavy adatoms such as Sn and Pb.

In this paper we perform a comprehensive theoretical description of magnetic properties in the Si(111):{C,Si,Sn,Pb} systems in the ground state as well as at finite temperatures and magnetic fields. Our approach combines first-principles simulations within density functional theory, construction of the low-energy models taking into account spin-orbit coupling and electronic correlations in the Wannier function basis, and determination of the magnetic exchange interactions by means of the superexchange theory. The zero-temperature mean-field Hartree-Fock solution of the constructed electronic models for the 3 × 3 unit cell reveals noncollinear 120°-Néel states for the adatom systems with carbon, silicon, and tin, while the 120°-row-wise magnetic state is found to be more stable in Si(111):Pb. Here, we argue that the formation of a magnetic order in the Si(111):X systems is a joint effect of spin-orbit coupling, direct exchange interactions between neighboring Wannier functions, and hopping parameters beyond nearest neighbors.

Another important result we obtained by means of classical Monte Carlo simulations is the complex spin patterns, such as interpenetrating spin spirals stabilized in the Si(111):{Sn,Pb} systems at low temperatures. These nontrivial structures are formed due to strong Dzyaloshinskii-Moriya interactions (DMIs) between nearest neighbors on a triangular lattice and, in principle, can be experimentally observed by using spin-polarized scanning tunneling microscopy [13,14]. Finally, at high magnetic fields ∼$2J_{01}$, where J_{01} is the isotropic exchange interaction between nearest neighbors, we predict the stabilization of an antiferromagnetic skyrmion lattice state.

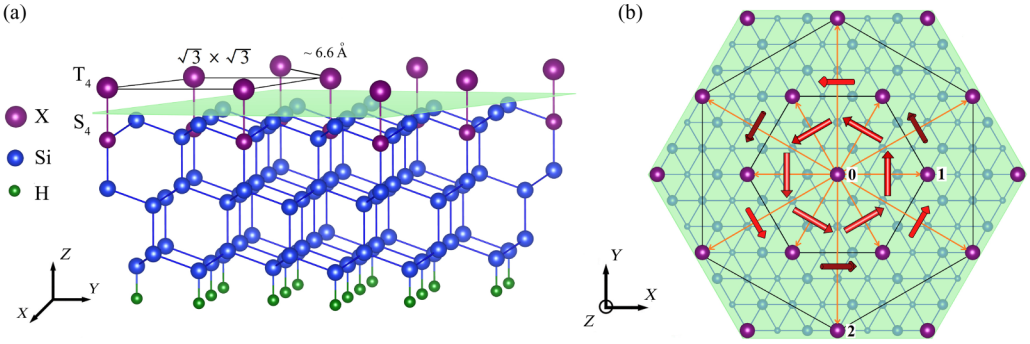

FIG. 1. (a) Crystal structure of Si(111):X. Violet spheres denote T_4-S_4 positions of adatoms X, and blue and green spheres show the silicon and hydrogen atoms, respectively. (b) xy plane. The interaction paths are shown with orange lines. Red arrows stand for the DMI vectors. For next-nearest-neighbor interactions dark and light red arrows denote the DMI vectors with the negative and positive z component, respectively. Crystal structures are visualized by using the VESTA software [12].

II. RESULTS OF DFT + SO CALCULATIONS

To simulate electronic and magnetic properties of the Si(111):{C,Si,Sn,Pb} systems, we have performed first-principles calculations within density functional theory (DFT) [15] using the generalized gradient approximation (GGA) with the Perdew-Burke-Ernzerhof (PBE) exchange-correlation functional [16]. To this end, we have employed Quantum Espresso [17] and Vienna *ab initio* simulation package (VASP) [18,19]. In these calculations, we set the energy cutoff in the plane-wave decomposition to 400 eV and the energy convergence criteria to 10^{-8} eV. For the Brillouin-zone integration a $20 \times 20 \times 1$ Monkhorst-Pack mesh was used.

The simulated atomic structures of the Si(111):{C,Si,Sn,Pb} systems are presented in Fig. 1 and contain three layers of silicon, one monolayer of adatoms, and a hydrogen slab, as described in Ref. [5]. Here, adatoms occupy the T_4 positions in Si/Si(111), Sn/Si(111), and Pb/Si(111) [6,9], while in the case of C/Si(111) adatoms are in the S_4 underlayer positions [20]. The optimized atomic structures are consistent with those reported in previous studies [6,9,20].

Band structures calculated within DFT demonstrate the main peculiarity of the systems, which is one well-separated doubly degenerate band located near the Fermi level, that is further split when spin-orbit coupling (DFT + SO) is taken into account [Fig. 2(b)]. This splitting strongly depends on the adatom type and varies from 3.5 meV (for C) to 109 meV (for Pb). Thus, within this family of the surface nanostructures one can probe either weak or strong limits of spin-orbit coupling in a strongly correlated material.

III. WANNIER FUNCTIONS

To parametrize the DFT + SO spectra and construct the corresponding low-energy models we have employed maximally localized Wannier functions [21–23]. As shown in Fig. 3, the resulting Wannier functions are strongly delocalized. Importantly, they are not centered at the adatoms. Instead, their centers are found to be close to the substrate plane. The spread of the Wannier functions in Si(111):{C,Si,Sn,Pb} (Table I) is much larger than those one observes in 3*d* transition metal compounds with strong hybridization effects (the corresponding spread in a copper oxide is about 4.5 Å^2) [24].

From Fig. 3 one can see that the structure of the constructed Wannier functions is very complicated. Previously, it was proposed that the separated band at the Fermi level is formed by molecular orbitals as a linear combinations of atomic orbitals of the adatom and substrate [6]. As we will show below, the delocalization of the magnetic orbitals leads to an additional ferromagnetic contribution to the total exchange interaction between nearest neighbors.

IV. SPIN AND ORBITAL MAGNETIZATION

Strong delocalization of the Wannier functions described in the previous section affects the magnetic properties of the systems in question. In this section we analyze and discuss the formation of the magnetic moments. For this purpose we use the results obtained from the spin-polarized DFT + SO calculations for the minimal ($\sqrt{3} \times \sqrt{3}$) unit cell, which corresponds to the case of the ferromagnetic configuration.

Due to the strong hybridization between the adatom and surface states, the total spin magnetic moment of the unit cell is considerably suppressed in the case of the Sn and Pb systems (Table I). Moreover, in the case of C/Si(111) the carbon adatom is in the S_4 underlayer position, and as a result the considerable spin (electron) density is concentrated on the substrate silicon atom Si1, which can be now considered as an effective adatom. The adatom contribution to the total magnetization gradually decreases within the series, ∼16% for Si/Si(111) and ∼6% for Pb/Si(111).

The calculated total and adatom magnetic moments in the Sn/Si(111) system are in good agreement with previous results reported in Ref. [9]. However, it is also important to compare their values with those calculated for closely related surface nanostructures. For instance, in the case of SiC(0001) [25] and Ge(111) surfaces [26] the spin magnetic moments of the Sn adatom are larger than that in Sn/Si(111) (this work). As shown in Ref. [27], the difference in magnetization between Sn/SiC(0001) and Sn/Si(111) can be explained by a more localized behavior of the system with the SiC substrate. The corresponding LDA bandwidth is about 0.5 eV for Sn/Si(111) and 0.29 eV for Sn/SiC(0001) [27].

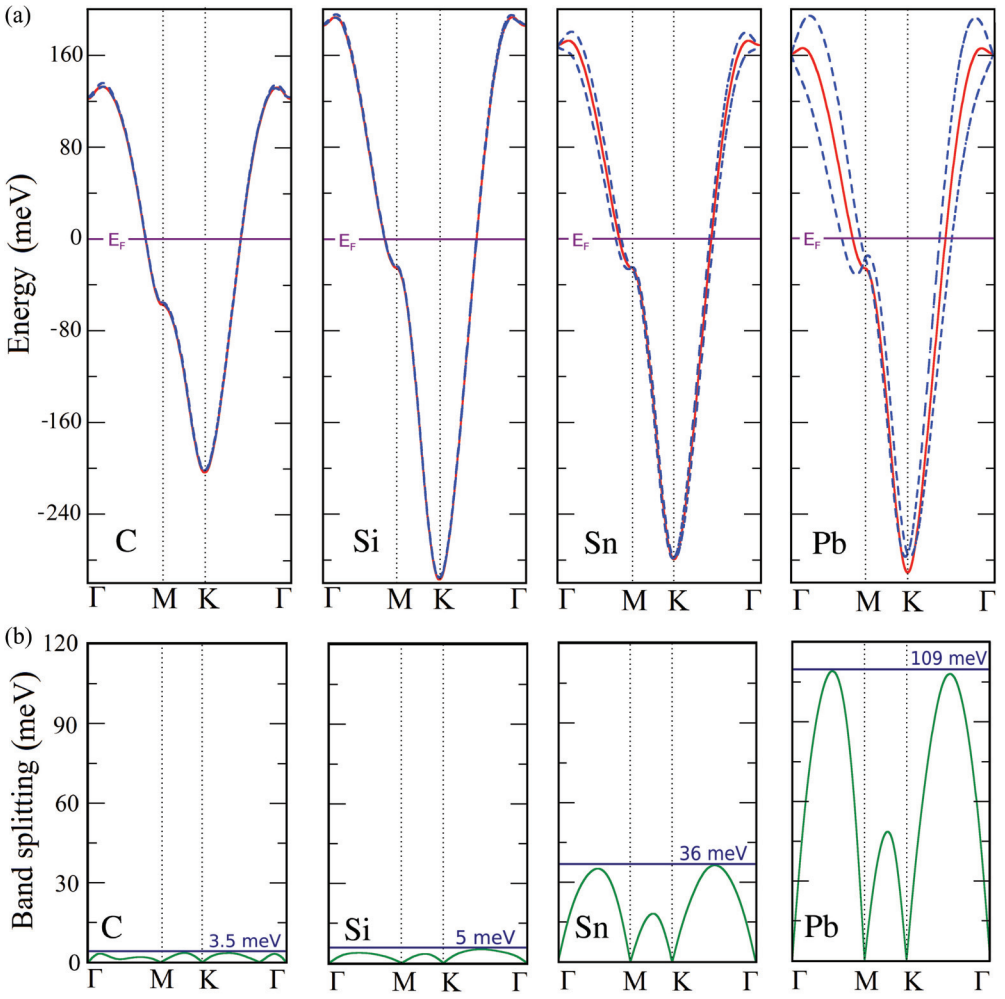

FIG. 2. (a) Band structures of Si(111):{C,Si,Sn,Pb} near the Fermi level as obtained from DFT (red solid line) and DFT + SO (blue dashed line) calculations. (b) Band splitting (in meV) due to spin-orbit coupling.

According to our first-principles calculations, the Si(111):{C,Si,Sn,Pb} surface nanostructures are characterized by a strong spin-orbit coupling. The p_z atomic orbital of adatoms (the head of the magnetic orbital) corresponds to zero angular momentum $L = 0$ and as a result gives zero orbital magnetization. However, since in our case the Wannier functions have a more complicated structure, one can expect a nonzero orbital magnetic moment as described in Ref. [28]. To this end we have performed calculations based on the modern theory of orbital magnetization implemented in the Quantum Espresso and Wannier 90 packages [29,30]. In these calculations we use a minimal $(\sqrt{3} \times \sqrt{3})$ unit cell with the ferromagnetic order. It was found that the orbital magnetization is close to zero ($\sim 10^{-3}\ \mu_B$) for all the systems in question. In the case of the Pb adatom we obtained $2.6 \times 10^{-3}\ \mu_B$ per unit cell. These results were confirmed by the direct calculation of the orbital magnetic moments of the atoms and unit cell by using VASP. They are also close to zero. Thus one can conclude that the g factor has no orbital contribution and $g \approx 2$. This result will be used in Sec. VIII to estimate critical magnetic fields needed to form a skyrmion state.

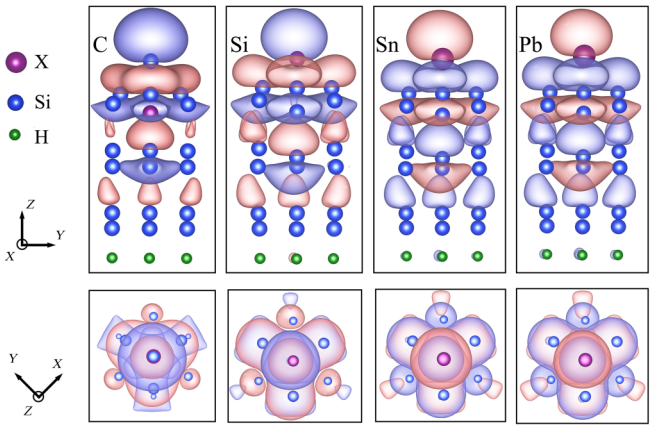

FIG. 3. Maximally localized Wannier functions describing the band at the Fermi level in Si(111):X with X = {C, Si, Sn, Pb}. Violet spheres denote adatoms.

V. LOW-ENERGY MODEL

To describe electronic and magnetic properties of the adatom systems we use an effective electronic model taking into account spin-orbit coupling and electronic correlations in

TABLE I. Bare direct exchange interactions and spreads of the Wannier functions (WF) calculated for the adatom systems Si(111):X with X = {C, Si, Sn, Pb}. M_S^{unit} and M_S^{adatom} are the total spin magnetization of the $\sqrt{3}\times\sqrt{3}$ unit cell and spin magnetic moment of the adatom as obtained from the spin-polarized DFT + SO calculations for the ferromagnetic state. The last two rows show the magnetic moments of the silicon atoms nearest and next nearest to the adatom.

X	C	Si	Sn	Pb
$J_{01}^{F\,(\text{bare})}$ (meV)	1.64	3.81	5.44	7.34
Spread of WF (Å^2)	12.4	15.6	16.8	17.7
M_S^{unit} (μ_B)	0.99	0.70	0.27	0.20
M_S^{adatom} (μ_B)	0.078	0.112	0.026	0.012
M_S^{Si1} (μ_B)	0.124	0.013	0.008	0.007
M_S^{Si2} (×3) (μ_B)	0.054	0.090	0.039	0.033

the Wannier function basis:

$$\hat{\mathcal{H}} = \sum_{ij,\sigma\sigma'} t_{ij}^{\sigma\sigma'} \hat{a}_{i\sigma}^{+}\hat{a}_{j\sigma'} + \frac{1}{2}\sum_{i,\sigma\sigma'} U\,\hat{a}_{i\sigma}^{+}\hat{a}_{i\sigma'}^{+}\hat{a}_{i\sigma'}\hat{a}_{i\sigma} + \frac{1}{2}\sum_{ij,\sigma\sigma'} V_{ij}\,\hat{a}_{i\sigma}^{+}\hat{a}_{j\sigma'}^{+}\hat{a}_{j\sigma'}\hat{a}_{i\sigma} + \frac{1}{2}\sum_{ij,\sigma\sigma'} J_{ij}^{F}\,\hat{a}_{i\sigma}^{+}\hat{a}_{j\sigma'}^{+}\hat{a}_{i\sigma'}\hat{a}_{j\sigma}, \quad (1)$$

where i (j) and σ (σ') are site and spin indices; U, V_{ij}, and J_{ij}^F represent the local Coulomb, nonlocal Coulomb, and direct exchange interactions, respectively; $t_{ij}^{\sigma\sigma'}$ is the element of the hopping matrix with spin-orbit coupling.

Coulomb and direct exchange interactions. The detailed analysis of the local and nonlocal Coulomb interactions in the Si(111):X systems was reported in Ref. [5]. It was found that the screened Coulomb interactions calculated within the random phase approximation (RPA) are about 4–5 times smaller than the bare ones. In our work we use their partially screened values as reported in Ref. [5]: $U = 1.4$, 1.1, 1.0, and 0.9 eV for C, Si, Sn, and Pb adatoms, respectively, and $V_{01} = 0.5$ eV for all adatoms.

In contrast to previous studies our model contains ferromagnetic exchange interactions as a result of the direct overlap between neighboring Wannier functions. To estimate an upper bound of J_{ij}^F, which corresponds to its bare value, we performed numerical integrations of the following expression by means of the Monte Carlo method:

$$J_{ij}^{F\,(\text{bare})} = \int \frac{W_i^*(\boldsymbol{r})W_j(\boldsymbol{r})W_j^*(\boldsymbol{r}')W_i(\boldsymbol{r}')}{|\boldsymbol{r}-\boldsymbol{r}'|} d\boldsymbol{r}d\boldsymbol{r}', \quad (2)$$

where $W_i(\boldsymbol{r})$ is a Wannier function centered at the ith site. The results are presented in Table I. One can see that the calculated values of $J_{ij}^{F\,(\text{bare})}$ are much smaller compared to the Coulomb interactions. However, as we will show below, they play an important role in magnetic properties of Si(111):{C,Si,Sn,Pb}.

Due to the smallness of J_{ij}^F, direct calculations of its partially screened value within RPA is a hard numerical problem requiring extremely accurate integrations. To give a reasonable estimation of the partially screened direct exchange interaction we use the ratio between bare and partially screened values of the Coulomb interaction parameters obtained in Ref. [5], which is about 4.5. Using the scaling relation $J_{01}^F = J_{01}^{F\,(\text{bare})}/4.5$, one obtains $J_{01}^F = 0.36$, 0.85, 1.21, and 1.63 meV for C, Si, Sn, and Pb adatoms, respectively. However, since the determination of J_{01}^F is a delicate task, we will also use J_{ij}^F as a free parameter for description of the ground (Sec. VI) and excited (Sec. VII) states of Si(111):{C,Si,Sn,Pb} by varying its value from zero to its bare limit.

TABLE II. Hopping integrals (in meV) between nearest and next-nearest neighbors as obtained from DFT + SO calculations for the adatom systems Si(111):X with X = {C, Si, Sn, Pb}. See Fig. 1(b) for details.

X	t_{01}	t_{02}
C	$\begin{pmatrix} 35.11 & 0.27 \\ -0.27 & 35.11 \end{pmatrix}$	$\begin{pmatrix} -13.47+0.14i & -0.43i \\ -0.43i & -13.47-0.14i \end{pmatrix}$
Si	$\begin{pmatrix} 48.33 & 0.71 \\ -0.71 & 48.33 \end{pmatrix}$	$\begin{pmatrix} -20.28+0.09i & -0.21i \\ -0.21i & -20.28-0.09i \end{pmatrix}$
Sn	$\begin{pmatrix} 43.51 & 5.53 \\ -5.53 & 43.51 \end{pmatrix}$	$\begin{pmatrix} -18.99+0.14i & -0.86i \\ -0.86i & -18.99-0.14i \end{pmatrix}$
Pb	$\begin{pmatrix} 41.32 & 16.68 \\ -16.68 & 41.32 \end{pmatrix}$	$\begin{pmatrix} -19.15+0.11i & -2.09i \\ -2.09i & -19.15-0.11i \end{pmatrix}$

Hopping integrals. The calculated hopping integrals are presented in Table II. Their diagonal parts are in excellent agreement with previously reported values obtained without spin-orbit coupling [5]. However, the latter gives a significant contribution that results in comparably large anisotropic exchange parameters. The structure of the hopping matrices in the spin space fully obeys the symmetry of the system. One can see that t_{01} is real and contains nondiagonal elements, which is a result of the C_{3v} symmetry of the triangular lattice formed by the Wannier functions (Fig. 4). For the next-nearest-neighbor bonds the symmetry is lower. We will analyze these symmetry aspects below on the level of the spin model.

VI. HARTREE-FOCK SIMULATIONS OF THE ELECTRONIC MODELS

Computational methods combining first-principles band structure calculations and many-body techniques are of great

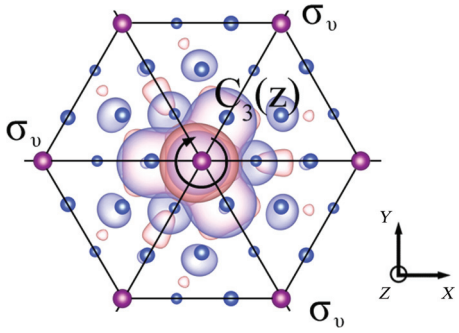

FIG. 4. C_{3v} symmetry of the triangular lattice formed by the Wannier functions. Here, $C_3(z)$ and σ_v stand for the rotation by $2\pi/3$ around the z axis and vertical mirror planes, respectively. Blue and violet spheres denote substrate silicon atoms and adatom, respectively.

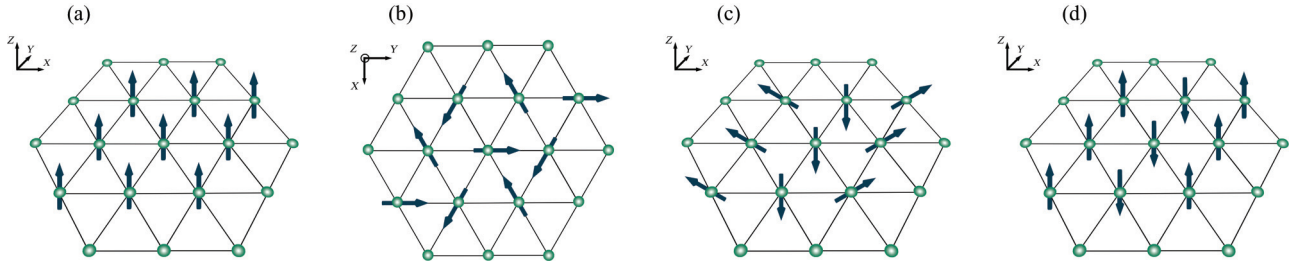

FIG. 5. Schematic view of magnetic structures used in the Hartree-Fock calculations: (a) ferromagnetic (FM), (b) 120°-Néel, (c) 120°-RW, and (d) collinear-RW.

interest in the physics of strongly correlated materials. Conventional approaches based on density functional theory (DFT) have the well-known difficulties related to a proper treatment of electronic correlations. On the other hand, their extensions taking into account correlations beyond DFT [such as DFT + U and dynamical mean-field theory (DMFT)] become really involved when a magnetic ground state and spin-orbit coupling effects are concerned.

For example, geometric frustrations and their interplay with electronic correlations have been the subject of intense research. In this context, the class of adatom systems Si(111):X is an ideal candidate to study these effects. It is known that the Hubbard model at half filling on a triangular lattice displays a 120° noncollinear ordering (120°-Néel). However, this point is not verified for the Si(111):Sn system, where early *ab initio* simulations in the weakly correlated regime showed that the 120°-Néel order is indeed stabilized in the Si(111):Sn system [2,9], while other studies based on the DMFT approach argued that an unusual collinear row-wise (RW) alignment takes place and emerges from long-range electron hopping processes [7,8]. Generally, a geometrically frustrated arrangement may destroy any long-range magnetic configuration and give rise to a spin-liquid state.

The problem gets even more complicated when electrons are delocalized. This issue was studied in Ref. [9] for the Si(111):Sn system, where local magnetic moments residing on Sn adatoms were shown to be small ($\sim$0.06 μ_B) compared to the total ferromagnetic moment. As shown in Table I, this takes place in all four systems. Thus, the magnetism in Si(111):X is far from being purely local and has a significant nonlocal character, so the picture of localized atomic magnetic moments used in DFT calculations seems to be inappropriate.

To tackle these problems one has to resort to a proper theoretical method. To this end, the basis of Wannier functions seems to be a more appropriate choice compared to that of atomic orbitals, as it incorporates hybridization effects and can serve as an alternative basis for the low-energy model. Indeed, as seen in Fig. 3, the resulting Wannier functions constructed by projecting a single band located near the Fermi level onto adatom p_z orbitals have a rather complicated structure and are spread in space quite significantly. Nonetheless, this choice allows us to work in the framework of localized magnetic moments, which in this case reside on the corresponding Wannier functions rather than on a single atomic orbital.

The effective model Eq. (1) constructed in the basis of Wannier functions is solved in the mean-field Hartree-Fock approximation, which has proved to be a good tool to study magnetic states in systems with strong correlations:

$$\left(\hat{t}_{\boldsymbol{k}} + \hat{\mathcal{V}}^H_{\boldsymbol{k}} + \hat{\mathcal{J}}^H_{\boldsymbol{k}}\right)|\varphi_{\boldsymbol{k}}\rangle = \varepsilon_{\boldsymbol{k}}|\varphi_{\boldsymbol{k}}\rangle, \tag{3}$$

where $\hat{t}_{\boldsymbol{k}}$ is the Fourier transform of the hopping parameters $\hat{t}_{ij}$, $\hat{\mathcal{V}}^H_{\boldsymbol{k}}$ and $\hat{\mathcal{J}}^H_{\boldsymbol{k}}$ are the Hartree-Fock potentials describing the on-site and intersite Coulomb and direct exchange interactions, respectively, and $\varepsilon_{\boldsymbol{k}}$ and $|\varphi_{\boldsymbol{k}}\rangle$ are the corresponding eigenvalues and eigenvectors in a given basis; a self-consistent solution of Eq. (3) is achieved with respect to the density matrix:

$$\hat{n} = \sum_{\boldsymbol{k}} |\varphi_{\boldsymbol{k}}\rangle\langle\varphi_{\boldsymbol{k}}|. \tag{4}$$

Further details on the computational scheme are provided in Refs. [31,32].

We have considered four possible magnetic configurations shown in Fig. 5 by comparing their energies calculated within the Hartree-Fock approximation for the unit cell containing nine correlated sites. As a first step, we neglect the direct exchange interaction J^F_{01} and take into account only Coulomb interactions U and V_{01} in Eqs. (1) and (3). From the corresponding energies presented in Table III it is seen that the 120°-Néel order is found to be dominating in Si(111):{C,Si,Sn}, while the 120°-RW order is more favorable in Si(111):Pb.

First, it is worth noting that the 120°-RW magnetic structure [Fig. 5(c)] is different from the collinear ferrimagnetic order [collinear row-wise magnetic structure; Fig. 5(d)] considered in previous studies [7,8]. The collinear row-wise order is unstable in our Hartree-Fock simulations for all the systems in question. The geometrical frustrations and spin-orbit coupling tend to align magnetic moments to form a 120° structure in the xz plane.

Second, the 120°-Néel order in X = Sn is in agreement with previous studies based on DFT + U calculations, while the DMFT-based approaches predict RW to be a magnetic

TABLE III. Energy of magnetic configurations (in eV with respect to the ferromagnetic state) in Si(111):X, X = {C, Si, Sn, Pb}, as calculated from the Hartree-Fock approximation for the 3 × 3 unit cell with $J^F_{01} = 0$ eV.

	Si(111):C	Si(111):Si	Si(111):Sn	Si(111):Pb
FM	0.0	0.0	0.0	0.0
120°-Néel	**−0.055**	**−0.149**	**−0.141**	−0.136
120°-RW	−0.042	−0.120	−0.124	**−0.143**

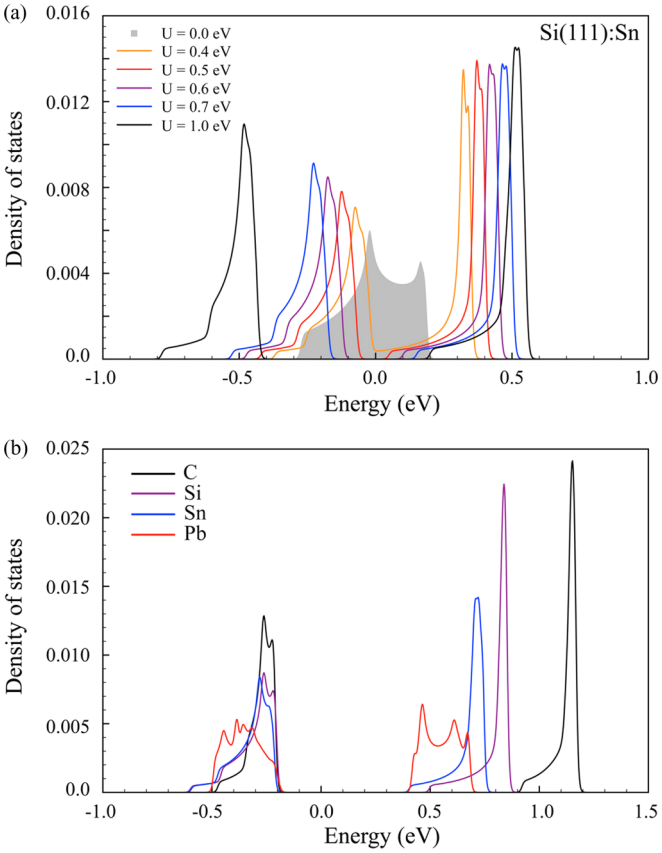

FIG. 6. (a) Densities of states in Si(111):Sn as obtained from the Hartree-Fock approximation for the 120°-Néel magnetic order with different values of U ($V_{01} = 0$, $J_{01}^F = 0$). (b) Densities of states corresponding to the magnetic ground states of Si(111):X, X = {C, Si, Sn, Pb} as obtained from the Hartree-Fock approximation in the full model, Eq. (1) [see Sec. V and Fig. 7(a)].

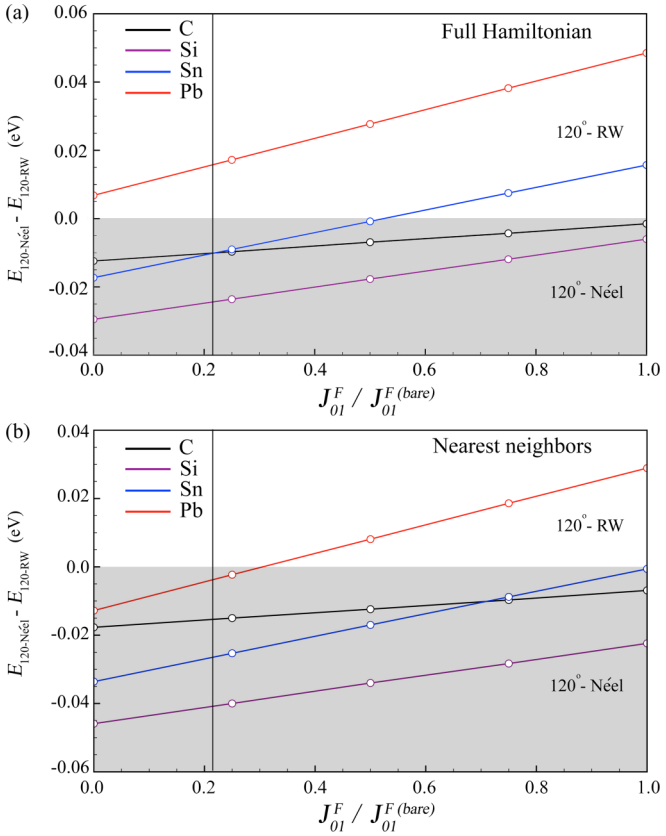

FIG. 7. Magnetic ground states for different values of J^F as obtained from the Hartree-Fock approximation (a) for the full model and (b) for the model with nearest-neighbor hopping parameters only. The ratio $J_{01}^F/J_{01}^{F\,(\mathrm{bare})} \approx 0.22$ given in Sec. III is shown with vertical lines. The energies were calculated for the unit cell containing nine correlated sites.

ground state for sufficiently large values of U. First of all, this discrepancy can be attributed to the fact that the Hartree-Fock approximation is formulated at zero temperature, while previous studies based on DMFT have been performed in the experimentally accessible temperature range. Next, our model Eq. (1) is extended to include the effect of spin-orbit coupling, which in the case of Si(111):{Sn,Pb} gives a significant contribution renormalizing hopping parameters.

To give some comparison on different approaches, we have explored critical values of the on-site Coulomb interaction U in a metal-insulator phase transition. Densities of states of the Si(111):Sn system calculated within the Hartree-Fock approximation for different values of U ($V_{01} = 0$, $J_{01}^F = 0$) are shown in Fig. 6(a). As seen, the charge gap starts to open at $U_c \approx 0.5$ eV, which is smaller than the critical values $U_c \approx 0.60$, 0.65, and 0.75 eV obtained within the single-site DMFT, variational cluster, and dual fermion approaches, respectively [8,9]. Despite this fact, we believe that the Hartree-Fock approximation is still reliable since the values of U used in our calculations (see Sec. V) are much higher compared to the critical ones. However, even though we treat electronic correlations in a mean-field manner, they do play an important role in stabilizing a magnetic ground state in the Si(111):X system.

Next, we proceed to study the effect of the direct exchange interaction J_{01}^F on a magnetic ground state. The results obtained with respect to the ratio $J_{01}^F/J_{01}^{F\,(\mathrm{bare})}$ are presented in Fig. 7(a). One can see that for any value of $J_{01}^F/J_{01}^{F\,(\mathrm{bare})}$ the 120°-Néel order is found to be stable in X = C and Si, while the 120°-RW magnetic structure is stabilized only in X = Pb. The situation is different in the case of Si(111):Sn, where depending on the ratio $J_{01}^F/J_{01}^{F\,(\mathrm{bare})}$ both magnetic states can be realized. This result leads to a very interesting conclusion that the magnetic ground state in the Si(111):X systems is also controlled by the value of J_{01}^F.

Another important conclusion is that for small ratios $J_{01}^F/J_{01}^{F\,(\mathrm{bare})}$ the energy difference of the 120°-Néel and 120°-RW magnetic orders in the Pb/Si(111) system is about 2 meV per correlated orbital, which, as we will show below, is smaller than the anisotropic exchange interaction between nearest neighbors. Thus, small variations of the intersite exchange interaction J_{01}^F in the Hartree-Fock simulations for the Pb/Si(111) system can lead to a transition between these two antiferromagnetic states.

To get a deeper insight on this effect, we have eliminated hopping parameters beyond nearest neighbors and performed the same calculations with respect to the ratio $J_{01}^F/J_{01}^{F\,(\mathrm{bare})}$. As shown in Fig. 7(b), the 120°-Néel order is stabilized in all four

TABLE IV. Isotropic J_{ij} and anisotropic $\boldsymbol{D}_{ij}$ exchange interactions (in meV) in Si(111):X, X = {C, Si, Sn, Pb}, as obtained from DFT + SO calculations, Eqs. (6) and (7). See Fig. 1(b) for details.

X	J_{01}	$\boldsymbol{D}_{01}$	J_{02}	$\boldsymbol{D}_{02}$	J_{02}/J_{01}
C	2.38	(0.0, 0.042, 0.0)	0.26	(0.015, 0.0, −0.005)	0.11
Si	6.94	(0.0, 0.228, 0.0)	0.75	(0.015, 0.0, −0.005)	0.11
Sn	6.48	(0.0, 1.925, 0.0)	0.73	(0.065, 0.0, −0.010)	0.11
Pb	8.30	(0.0, 6.895, 0.0)	0.83	(0.180, 0.0, −0.009)	0.10

TABLE V. Symmetric anisotropic exchange interactions $\overleftrightarrow{\Gamma}_{01}$ (in meV) in Si(111):Sn and Si(111):Pb as obtained from DFT + SO calculations, Eq. (8). See Fig. 1(b) for details.

	Sn			Pb		
$\overleftrightarrow{\Gamma}_{01}$	0.0	0.0	0.0	0.0	0.0	0.0
	0.0	0.245	0.0	0.0	2.784	0.0
	0.0	0.0	0.0	0.0	0.0	0.0

systems, as expected for the nearest-neighbor Hubbard model on a triangular lattice. However, in this case the transition between the 120° Néel and 120°-RW magnetic orders is still observed in Si(111):Pb. As will be shown below, this direct exchange interaction gives an additional contribution to the kinetic isotropic exchange parameters between magnetic moments favoring their ferromagnetic alignment. Meanwhile, we conclude that the stabilization of a magnetic order in the Si(111):X systems is a joint effect of long-range hopping processes, spin-orbit coupling, and nonlocal electron correlations.

VII. SPIN HAMILTONIAN

To probe the excited magnetic states in the adatom systems we construct spin models within the superexchange theory [33] formulated in the limit $t_{ij} \ll U$. In our case t_{ij}/U varies from 0.025 (for X = C) to 0.045 (for X = Pb) that justifies this approach. The corresponding spin Hamiltonian is given by

$$\hat{\mathcal{H}}^{spin} = \sum_{ij} J_{ij}\hat{\boldsymbol{S}}_i\hat{\boldsymbol{S}}_j + \sum_{ij} \boldsymbol{D}_{ij}[\hat{\boldsymbol{S}}_i \times \hat{\boldsymbol{S}}_j] + \sum_{ij} \hat{\boldsymbol{S}}_i \overleftrightarrow{\Gamma}_{ij} \hat{\boldsymbol{S}}_j, \tag{5}$$

where $\hat{\boldsymbol{S}}$ is the spin operator, and J_{ij}, $\boldsymbol{D}_{ij}$, and $\overleftrightarrow{\Gamma}_{ij}$ are the isotropic exchange coupling, antisymmetric anisotropic (Dzyaloshinskii-Moriya), and symmetric anisotropic interactions, respectively. The summation runs twice over all pairs.

Isotropic exchange interaction. In terms of the electronic model parameters given in Eq. (1) the isotropic exchange interaction can be expressed in the following form [33,34]:

$$J_{ij} = \frac{1}{\widetilde{U}} \mathrm{Tr}_\sigma\{\hat{t}_{ji}\hat{t}_{ij}\} - J^F_{ij}, \tag{6}$$

where $\hat{t}_{ij}$ is the hopping integral with spin-orbit coupling, and the effective local Coulomb interaction is estimated as $\widetilde{U} = U - V_{ij}$. The first kinetic term is the famous Anderson's superexchange, while the second one, J^F_{ij}, represents the direct ferromagnetic exchange due to the overlap between neighboring Wannier functions. Their values calculated with the partially screened J^F_{ij} as described in Sec. V are given in Table IV.

Anisotropic exchange interactions. Antisymmetric Dzyaloshinskii-Moriya and symmetric anisotropic exchange interactions are given by

$$\boldsymbol{D}_{ij} = \frac{i}{2\widetilde{U}}[\mathrm{Tr}(\hat{t}_{ij})\mathrm{Tr}(\hat{t}_{ji}\boldsymbol{\sigma}) - \mathrm{Tr}(\hat{t}_{ji})\mathrm{Tr}(\hat{t}_{ij}\boldsymbol{\sigma})], \tag{7}$$

$$\overleftrightarrow{\Gamma}_{ij} = \frac{1}{2\widetilde{U}}[\mathrm{Tr}(\hat{t}_{ji}\boldsymbol{\sigma}) \otimes \mathrm{Tr}(\hat{t}_{ij}\boldsymbol{\sigma}) + \mathrm{Tr}(\hat{t}_{ij}\boldsymbol{\sigma}) \otimes \mathrm{Tr}(\hat{t}_{ji}\boldsymbol{\sigma})], \tag{8}$$

where $\boldsymbol{\sigma}$ are the Pauli matrices.

The calculated DMIs are presented in Table IV. Let us first discuss their symmetry. Since the resulting Wannier functions reside on the adatom-silicon bonds, symmetry properties of the spin Hamiltonian are consistent with the C_{3v} point group of a triangular lattice formed by adatoms. According to Moriya's rules [35], vertical reflections go through the bonds between nearest neighbors, and the corresponding anisotropic exchange parameters are perpendicular to their bonds and lie in the xy plane (see Fig. 4). On the other hand, next-nearest neighbors are not located on the mirror planes, and we obtain the nonzero z components of the anisotropic exchange parameters that alternate within the coordination sphere.

Another important contribution to the magnetic anisotropy is the symmetric anisotropic exchange interaction, $\overleftrightarrow{\Gamma}_{ij}$. The calculated tensors for the Si(111):Sn and Pb systems are presented in Table V. One can see that they favor alignment of the magnetic moments in the xz plane, and the principal axis of $\overleftrightarrow{\Gamma}_{01}$ coincides with the DMI vector for the same bond in agreement with the results of Ref. [36], where a general one-band Hubbard model with spin-orbit coupling was analyzed. The corresponding elements of $\overleftrightarrow{\Gamma}_{ij}$ for X = Si and C are less than 10^{-4} meV.

In the systems with inversion symmetry breaking the ratio $\frac{|\boldsymbol{D}_{ij}|}{J_{ij}}$ is a control parameter for the period of spiral structures or for a size of individual skyrmions at finite temperatures and magnetic fields. Depending on the adatom this ratio for the kinetic interactions presented in Table IV is varied from 0.017 (for X = C) to 0.83 (for X = Pb). It provides unprecedented possibilities to control and tune the DMI strength within this family of surface nanostructures.

Importantly, the spin Hamiltonians obtained for the adatom systems can be classified with respect to the ratio between the nearest-neighbor DMI, $\boldsymbol{D}_{01}$, and next-nearest-neighbor isotropic exchange interaction, J_{02}. For instance, in the case of the C/Si(111) and Si/Si(111) systems $J_{02} > |\boldsymbol{D}_{01}|$ and the corresponding spin model is the isotropic Heisenberg model of the J_{01}-J_{02} type. For the calculated ratio $\frac{J_{02}}{J_{01}} \approx 0.1$ presented in Table IV previous theoretical studies based on the classical J_{01}-J_{02} spin Hamiltonian have revealed the formation of the 120°-Néel state [37]. Namely, this state is observed in our zero-temperature simulations for the C/Si(111) and Si/Si(111) systems. Moreover, the calculated ratio $\frac{J_{02}}{J_{01}} \approx 0.1$ prevents the formation of any incommensurate spiral structure in the ground state as well as a skyrmion state at finite magnetic fields [38]. In turn, it is worth noting that solutions of the quantum J_1-J_2 spin models identify $\frac{J_{02}}{J_{01}} = 0.1$ as a transition point to the spin-liquid state [39,40].

The situation is different in the case of Sn/Si(111) and Pb/Si(111) where spin-orbit coupling has a noticeable effect

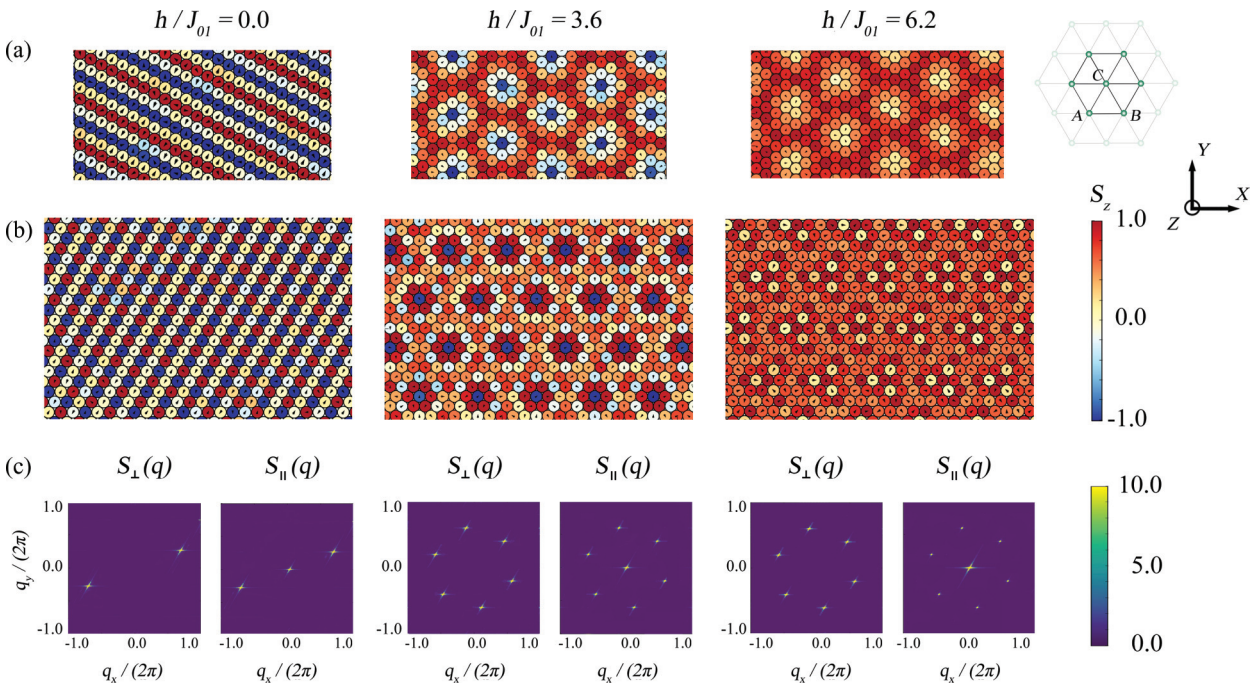

FIG. 8. Snapshots of the Si(111):Pb spin texture given for a sublattice A (a) and a full lattice (b) as obtained from Monte Carlo simulations for $N = 150 \times 150$, $T/J_{01} = 0.01$ and different values of h/J_{01}. Spin components in the xy plane are indicated with black arrows. (c) Static spin structure factors for the corresponding spin textures.

and J_{01} and $\boldsymbol{D}_{01}$ are of the same order and much larger than J_{02}. As a result, this property leads to the formation of a novel 120° row-wise order as shown in the previous section and antiferromagnetic skyrmion lattice states as we will show below.

VIII. MONTE CARLO RESULTS

In crystals with the C_{nv} symmetry, the anisotropic exchange interaction favors a rotation of magnetic moments along the propagation direction of a spin spiral structure, and they are expected to possess a Néel-type skyrmion state [41]. Moreover, the formation of an antiferromagnetic skyrmion texture (AF-SkX) on the antiferromagnetic triangular lattice with Dzyaloshinskii-Moriya interactions was reported recently [42].

In this section we focus on the effect of an external magnetic field $\boldsymbol{h}$ applied to the spin system Eq. (5):

$$\mathcal{H} = \mathcal{H}^{spin} - h\sum_i e_i^z, \tag{9}$$

where the spin variables are now treated as classical vectors, $|\boldsymbol{e}_i| = 1$, and the magnetic field is directed along the z axis. In a classical limit for the given spin vector length one has to renormalize model parameters of the quantum spin model. This is done by scaling the exchange interactions (given in Tables IV and V) by the maximum length of the product of two spin operators, that is, $S(S+1)$, where $S = 1/2$ and $\hbar = 1$. However, it is worth noting that this scaling is rather arbitrary and instead of using unit vectors one can leave their quantum mechanical length without distinction between model parameters.

Our Monte Carlo simulations have been performed based on the heat-bath method combined with overrelaxation. The corresponding model parameters are given up to next-nearest neighbors. In these calculations supercells of various size from $N = 96 \times 96$ to 150×150 spins with periodic boundary conditions are used and a single run contains $(0.5–2.0) \times 10^6$ Monte Carlo steps. For initial relaxation the system is gradually cooled down from higher temperatures.

While different states can be identified from the real-space spin textures, to trace their formation we have computed the static spin structure factors:

$$S_\perp(\boldsymbol{q}) = \frac{1}{N}\left\langle \left|\sum_i e_i^x\, e^{-i\boldsymbol{q}\cdot\boldsymbol{r}_i}\right|^2 + \left|\sum_i e_i^y\, e^{-i\boldsymbol{q}\cdot\boldsymbol{r}_i}\right|^2 \right\rangle \tag{10}$$

and

$$S_\parallel(\boldsymbol{q}) = \frac{1}{N}\left\langle \left|\sum_i e_i^z e^{-i\boldsymbol{q}\cdot\boldsymbol{r}_i}\right|^2 \right\rangle, \tag{11}$$

as well as the total chirality χ_L and skyrmion number χ_Q:

$$\chi_L = \frac{1}{8\pi}\left\langle \sum_i \chi_i^{(12)} + \chi_i^{(34)} \right\rangle \tag{12}$$

and

$$\chi_Q = \frac{1}{8\pi}\left\langle \sum_i A_i^{(12)}\mathrm{sgn}\left[\chi_i^{(12)}\right] + A_i^{(34)}\mathrm{sgn}\left[\chi_i^{(34)}\right] \right\rangle, \tag{13}$$

where $\chi_i^{(ab)} = \boldsymbol{e}_i \cdot \boldsymbol{e}_a \times \boldsymbol{e}_b$ is the so-called local chirality defined on a triangle $\{\boldsymbol{r}_i, \boldsymbol{r}_a, \boldsymbol{r}_b\}$ and $A_i^{(ab)} = \| (\boldsymbol{e}_a - \boldsymbol{e}_i) \times (\boldsymbol{e}_b - \boldsymbol{e}_i) \| /2$ is the corresponding area. The latter quantities

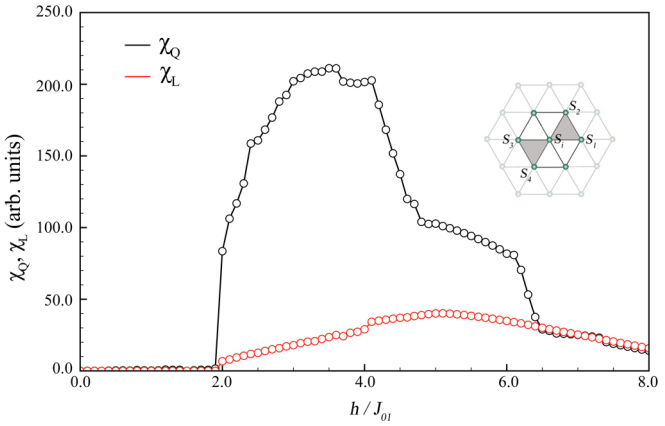

FIG. 9. Skyrmion number χ_Q and total chirality χ_L as a function of the applied magnetic field h/J_{01} obtained from the Monte Carlo simulations for $N = 150 \times 150$ and $T/J_{01} = 0.01$ in Si(111):Pb. The inset shows the corresponding area used to calculate local chiralities, Eqs. (10)–(11).

are considered as order parameters that represent topological stability of the corresponding state.

First, it is important to demonstrate connection between the finite-temperature Monte Carlo and zero-temperature Hartree-Fock results. To this end we performed Monte Carlo simulations for the 3×3 unit cell. The obtained magnetic configurations are of 120°-Néel or 120°-RW type in agreement with the Hartree-Fock approximation [Fig. 7(a)]. We would like to stress that such a small size of the unit cell prevents the formation of any long-range magnetic order. We address this question below.

The results obtained for the Si(111):Pb system for the 150×150 unit cell are presented in Fig. 8. Interestingly, the system exhibits several phases as a magnetic field applied along the z axis is varied. At low magnetic fields a complex spin spiral state is stabilized. It is composed of three interpenetrating spin spirals formed on each sublattice and characterized by a single $\boldsymbol{q}$ vector. As the magnetic field increases the system enters into a stable AF-SkX state which is a superposition of three Néel-type SkX lattices characterized by three q vectors (which are in turn formed by three spin spirals). As seen from Fig. 9, the AF-SkX state is favored in a wide range of magnetic fields. However, a stepwise behavior of the skyrmion number and total chirality with respect to the magnetic field is a result of the discrete finite-size model allowing for only definite numbers of skyrmions [42]. Finally, at higher magnetic fields the AF-SkX state is followed by a vortex-like texture and a paramagnetic phase. We observe a weak dependence of $|\boldsymbol{q}|$ on the magnetic field as one can see from Fig. 8(c), for instance, $|\boldsymbol{q}| = 0.76$ ($h = 0.0$), $|\boldsymbol{q}| = 0.76$ ($h = 3.6J_{01}$), and $|\boldsymbol{q}| = 0.59$ ($h = 6.2J_{01}$).

Our results are in agreement with those reported in Ref. [42]. However, it is worth mentioning that in this work we have employed an extended spin model including both antisymmetric and symmetric anisotropy terms up to the next-nearest neighbors, which justifies the realization of the so-called multiple $\boldsymbol{q}$ states in a more general case. The similar skyrmion lattice state is realized in Sn/Si(111). However, there is one important difference, which is a skyrmion size controlled by the ratio $\frac{|\boldsymbol{D}_{ij}|}{J_{ij}}$ and estimated to be about 40 Å and 26 Å for X = Sn and Pb, respectively.

Finally, Fig. 9 gives us the value of the magnetic field $\sim 2J_{01}$ needed to form a skyrmion state. Taking the estimated g factor and calculated exchange interaction parameters we conclude that the critical point may be accessible at the magnetic fields $\sim$190 T for Sn/Si(111) and $\sim$250 T for Pb/Si(111), which is too large to be reached in laboratories. To decrease their values one can reduce isotropic exchange interactions between nearest neighbors. In our simulations it can be done by changing the value of J_{01}^F. For instance, if one takes its bare value $J_{01}^{F\,(\mathrm{bare})} = 5.44$ meV for Sn/Si(111) the critical field can be estimated as 66 T. On the other hand, one can consider a mixed adatom system combining carbon (weak isotropic exchange) and tin (strong Dzyaloshinskii-Moriya interaction) sublattices. This aspect remains open for future investigation.

IX. SUMMARY

The main purpose of our study is to complete the picture of principal interactions in the Si(111):{C,Si,Sn,Pb} adatom systems. Taking into account spin-orbit coupling leads to a complex nondiagonal form of the hopping matrix, while the overlap between neighboring Wannier functions is responsible for the direct ferromagnetic exchange interaction that strongly affects low-energy properties of the systems in question. Our solutions of the constructed electronic and spin models have shown that the resulting state of the surface nanosystem mainly depends on these parameters that can be varied with the adatom type and their coupling with a substrate.

ACKNOWLEDGMENTS

We acknowledge fruitful discussions with Igor Solovyev. The work is supported by the Ministry of Education and Science of the Russian Federation, Project No. 16.1751.2014/K, and President of Russian Federation Grant No. MD-6458.2016.2. M.I.K. acknowledges support from the ERC Advanced Grant 338957 FEMTO/NANO.

[1] S. Modesti, L. Petaccia, G. Ceballos, I. Vobornik, G. Panaccione, G. Rossi, L. Ottaviano, R. Larciprete, S. Lizzit, and A. Goldoni, Phys. Rev. Lett. **98**, 126401 (2007).
[2] G. Profeta and E. Tosatti, Phys. Rev. Lett. **98**, 086401 (2007).
[3] J. M. Carpinelli, H. H. Weitering, M. Bartkowiak, R. Stumpf, and E. W. Plummer, Phys. Rev. Lett. **79**, 2859 (1997).
[4] J. Slezák, P. Mutombo, and V. Cháb, Phys. Rev. B **60**, 13328 (1999).
[5] P. Hansmann, T. Ayral, L. Vaugier, P. Werner, and S. Biermann, Phys. Rev. Lett. **110**, 166401 (2013).
[6] P. Hansmann, L. Vaugier, H. Jiang, and S. Biermann, J. Phys.: Condens. Matter **25**, 094005 (2013).

[7] G. Li, P. Hopfner, J. Schafer, C. Blumenstein, S. Meyer, A. Bostwick, E. Rotenberg, R. Claessen, and W. Hanke, Nat. Commun. **4**, 1620 (2013).

[8] G. Li, M. Laubach, A. Fleszar, and W. Hanke, Phys. Rev. B **83**, 041104 (2011).

[9] S. Schuwalow, D. Grieger, and F. Lechermann, Phys. Rev. B **82**, 035116 (2010).

[10] P. Hansmann, T. Ayral, A. Tejeda, and S. Biermann, Sci. Rep. **6**, 19728 (2016).

[11] H. Fu, Z. Liu, C. Lian, J. Zhang, H. Li, J.-T. Sun, and S. Meng, Phys. Rev. B **94**, 035427 (2016).

[12] M. Koichi and F. Izumi, J. Appl. Crystallogr. **44**, 1272 (2011).

[13] R. Wiesendanger, Rev. Mod. Phys. **81**, 1495 (2009).

[14] N. Romming, A. Kubetzka, C. Hanneken, K. von Bergmann, and R. Wiesendanger, Phys. Rev. Lett. **114**, 177203 (2015).

[15] W. Kohn and L. J. Sham, Phys. Rev. **140**, A1133 (1965).

[16] J. P. Perdew, K. Burke, and M. Ernzerhof, Phys. Rev. Lett. **77**, 3865 (1996).

[17] P. Giannozzi, S. Baroni, N. Bonini, M. Calandra, R. Car, C. Cavazzoni, D. Ceresoli, G. L. Chiarotti, M. Cococcioni, I. Dabo, A. Dal Corso, S. de Gironcoli, S. Fabris, G. Fratesi, R. Gebauer, U. Gerstmann, C. Gougoussis, A. Kokalj, M. Lazzeri, L. Martin-Samos, N. Marzari, F. Mauri, R. Mazzarello, S. Paolini, A. Pasquarello, L. Paulatto, C. Sbraccia, S. Scandolo, G. Sclauzero, A. P. Seitsonen, A. Smogunov, P. Umari, and R. M. Wentzcovitch, J. Phys.: Condens. Matter **21**, 395502 (2009).

[18] G. Kresse and J. Hafner, Phys. Rev. B **47**, 558 (1993).

[19] G. Kresse and J. Furthmüller, Phys. Rev. B **54**, 11169 (1996).

[20] C. A. Pignedoli, A. Catellani, P. Castrucci, A. Sgarlata, M. Scarselli, M. De Crescenzi, and C. M. Bertoni, Phys. Rev. B **69**, 113313 (2004).

[21] N. Marzari and D. Vanderbilt, Phys. Rev. B **56**, 12847 (1997).

[22] I. Souza, N. Marzari, and D. Vanderbilt, Phys. Rev. B **65**, 035109 (2001).

[23] A. A. Mostofi, J. R. Yates, Y-S. Lee, I. Souza, D. Vanderbilt, and N. Marzari, Comput. Phys. Commun. **178**, 685 (2008).

[24] D. I. Badrtdinov, O. S. Volkova, A. A. Tsirlin, I. V. Solovyev, A. N. Vasiliev, and V. V. Mazurenko, Phys. Rev. B **94**, 054435 (2016).

[25] S. Yi, H. Lee, J.-H. Choi, and J.-H. Cho, Sci. Rep. **6**, 30598 (2016).

[26] J.-H. Lee, H.-J. Kim, and J.-H. Cho, Phys. Rev. Lett. **111**, 106403 (2013).

[27] S. Glass, G. Li, F. Adler, J. Aulbach, A. Fleszar, R. Thomale, W. Hanke, R. Claessen, and J. Schäfer, Phys. Rev. Lett. **114**, 247602 (2015).

[28] S. A. Nikolaev and I. V. Solovyev, Phys. Rev. B **89**, 064428 (2014).

[29] T. Thonhauser, D. Ceresoli, D. Vanderbilt, and R. Resta, Phys. Rev. Lett. **95**, 137205 (2005).

[30] D. Ceresoli, U. Gerstmann, A. P. Seitsonen, and F. Mauri, Phys. Rev. B **81**, 060409(R) (2010).

[31] I. V. Solovyev, J. Phys.: Condens. Matter **20**, 293201 (2008).

[32] S. A. Nikolaev, V. V. Mazurenko, A. A. Tsirlin, and V. G. Mazurenko, Phys. Rev. B **94**, 144412 (2016).

[33] P. W. Anderson, Phys. Rev. **115**, 2 (1959).

[34] T. Yildirim, A. B. Harris, A. Aharony, and O. Entin-Wohlman, Phys. Rev. B **52**, 10239 (1995).

[35] T. Moriya, Phys. Rev. **120**, 91 (1960).

[36] L. Shekhtman, O. Entin-Wohlman, and A. Aharony, Phys. Rev. Lett. **69**, 836 (1992).

[37] S. E. Korshunov, Phys. Rev. B **47**, 6165 (1993).

[38] T. Okubo, S. Chung, and H. Kawamura, Phys. Rev. Lett. **108**, 017206 (2012).

[39] R. Kaneko, S. Morita, and M. Imada, J. Phys. Soc. Jpn. **83**, 093707 (2014).

[40] Y. Iqbal, W.-J. Hu, R. Thomale, D. Poilblanc, and F. Becca, Phys. Rev. B **93**, 144411 (2016).

[41] A. N. Bogdanov and D. A. Yablonsky, Sov. Phys. JETP **95**, 178 (1989).

[42] H. D. Rosales, D. C. Cabra, and P. Pujol, Phys. Rev. B **92**, 214439 (2015).